Organic Electronics 96 (2021) 106257

Contents lists available at ScienceDirect

Organic Electronics

journal homepage: www.elsevier.com/locate/orgel

Balanced shelf and operational stability of the PM6:Y6 solar cells by using ZnO:PEI composite electron transporting layer

Mingyue Li [a,b], Wusong Zha [a,b], Yunfei Han [a,b], Bowen Liu [a,b], Qun Luo [a,b,*], Chang-Qi Ma [a,b,**]

[a] School of Nano-Tech and Nano-Bionics, University of Science and Technology of China, Hefei, 230026, PR China
[b] Printable Electronics Research Center, Suzhou Institute of Nano-Tech and Nano-Bionics, Chinese Academy of Sciences, Suzhou, 215123, PR China

ARTICLE INFO

Keywords:
Organic solar cells
Electron transporting layer
Long-term stability
Shelf stability
ZnO:PEI composite

ABSTRACT

The operational stability under continuous illumination and the shelf stability in air are all important for the real application of the organic solar cells (OSCs). In this work, we investigated the influence of the commonly used electron transporting layer (ETL), *i. e.* ZnO and polyethyleneimine (PEI) on the shelf and operational stability of the PM6:Y6 OSCs. Due to the photocatalysis effect of ZnO, the operational stability of ZnO ETL-based device is worse than the PEI ETL-based device. Due to the hygroscopicity of PEI, the shelf stability of the PEI ETL-based device is worse than the ZnO ETL-based device. By using a ZnO:PEI composite ETL, a balanced shelf and operational stability was obtained. For the inverted PM6: Y6 solar cells, the device could remain 80% and 60% of the initial efficiency after 1200 h continuous illumination, and storage in air for 1500 h, respectively.

1. Introduction

Organic solar cells (OSCs) have several advantages of light weight, solution processing and semitransparency [1–3], showing extensive application prospect. Non-fullerene organic solar cells have achieved significant development over recent ten years. Recently, the efficiency of non-fullerene single-junction cells has reached above 18% [4]. Nowadays, device stability shows as a critical issue that decides the real application of organic solar cells [5]. To improve the efficiency and stability, many efforts were taken to develop new donor, acceptor [6], and interfacial material [7], develop interface modification [8] and phase separation morphology regulation strategy. Among the above aspects, the interfacial layer can significantly impact the OSCs stability due to interface chemical reaction [9].

ZnO is the most commonly used electron transport layer (ETL) in non-fullerene solar cells because of its low cost, easy preparation and environmental friendliness [10]. However, previous works found ZnO would cause photoinduced degradation of organic materials [11], which could result in a quick degradation. To solve this problem, the ZnO films should be modified by surface modification or compositing with other materials. Ma et al. [12] treated ZnO surface with hydroxide or hydroxyl scavengers to restrain the generation of hydroxyl radicals so that they improved the stability of the OSCs. Sankara et al. [13] used rGO and ZnO nanocomposite as an ETL to improve the charge extraction properties. Besides ZnO, polyethyleneimine (PEI) is also a promising candidate for the electron transport layer in the organic solar cells. PEI is a non-conjugated polymer with low work function. It is often coated between the high work function electrode and the semiconducting layers as a surface modifier to greatly reduce the work function of metals, transparent conductive metal oxides, conductive polymers and graphene [14–16]. Sadeghianlemraski et al. used PEI instead of ZnO in fullerene solar cells to maintain the charge selectivity of the electron-collecting contacts and greatly reduce the open-circuit voltage (V_{OC}) loss of OSCs [17,18]. However, PEI may react as a nucleophile with the C═O moiety of the non-fullerene acceptor small molecule and prevent the intramolecular charge transfer [19]. The reaction between PEI and acceptor is associated with the structure of acceptor. Composite buffer layers containing metal oxides and polymer showed several advantages of improved film quality, higher working thicknesses, and higher printing compatibility. Zhan et al. [20] used an ethoxylated polyethyleneimine (PEIE) modification layer to make flexible and better bending resistance non-fullerene all-plastic devices. Seong-Geun et al.

* Corresponding author. Printable Electronics Research Center, Suzhou Institute of Nano-Tech and Nano-Bionics, Chinese Academy of Sciences, Suzhou, 215123, PR China.
** Corresponding author. Printable Electronics Research Center, Suzhou Institute of Nano-Tech and Nano-Bionics, Chinese Academy of Sciences, Suzhou, 215123, PR China.
E-mail addresses: qluo2011@sinano.ac.cn (Q. Luo), cqma2011@sinano.ac.cn (C.-Q. Ma).

https://doi.org/10.1016/j.orgel.2021.106257
Received 1 April 2021; Received in revised form 19 May 2021; Accepted 16 June 2021
Available online 19 June 2021

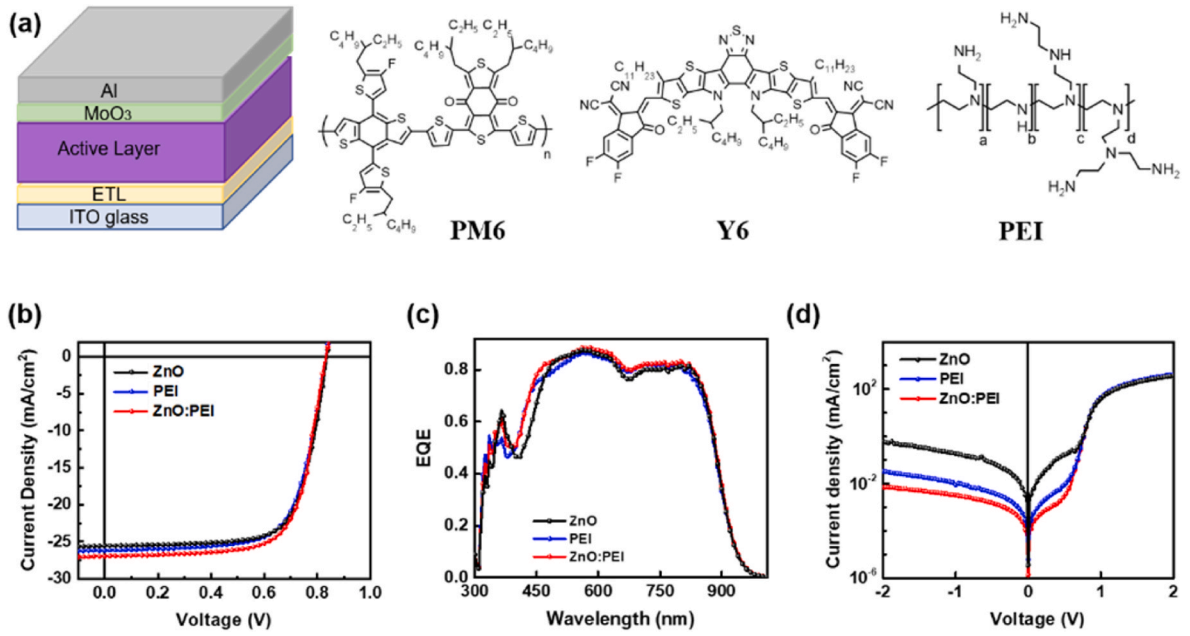

Fig. 1. (a) The inverted device structure and molecule structures of PM6, Y6, PEI (b) *J-V* curves, (c) EQE spectra and (d) *J-V* dark curves of the PM6:Y6 solar cells with ZnO, PEI, ZnO:PEI as the ETL.

used a PEI-ZnO complex colloid containing 2-(2-methoxyethoxy) acetic acid (MEA) organic dispersant. The addition of PEI reduced the work function of the ZnO colloid, completed the gaps in the ZnO coating layer, and made the surface smoother, resulting in the enhancement of the devices short circuit current (J_{SC}) and fill factor (FF) [21]. ZnO:PEI composite layer could also be used in large-scale roll-to-roll micro-gravure printing as a thickness insensitive electron transport layer. With the composite of PEI, the ink stability and the film mechanical property were improved [22]. ZnO:PEI composite based device showed superior fill factor and wide tolerance of layer thickness [23]. Regarding the device stability, Zhou et al. [19,24] found that the non-fullerene receptor Y6 material had good chemical stability with amine and use PEI chelated with Zn^{2+} as the interfacial layer material of ultra-flexible solar cells, which had the excellent bending ability [25].

In terms of device stability, both the operational stability under continuous illumination and the storage stability in air are important for practical application. The former decided the function of devices during the long-term working process, and the latter decided the convenience during business transport. Therefore, synergetic considerations on shelf stability and operational stability are necessary. Most of the works focused on the working stability. Several works demonstrated the shelf stability was influenced by the interfacial layer and the photoactive layer. Ameri et al. [26] designed a ternary device of PBDB-TF:IT-4F with 5% ICMA to enhance air stability in the dark. Ma et al. [27] found addition of 1,8-diiodooctane (DIO) would influence the work stability and air stability. Besides, Tang et al. [28] developed a porous ZnO/PEIE (P–ZnO) hybrid material as ETL for the P–ZnO/PBDB-T/DTPPSe-2F-based device. It presented a long-term storage stability, that maintaining 85% PCE in ambient air-condition without encapsulation for 1000 h. Similarly, Chen et al. [29] used polyolefin elastomer (POE) as anode interfacial layer instead of MoO_3, and the PM6:IT-4F device maintained 80.8% of the initial PCE after storage in air for 150 h when the humidity was approximately 70%. However, few works have been reported on the systematic research on operational and shelf stability.

In this work, we investigated the influence of ETL on the shelf and operational stability of the inverted OSCs. ZnO and PEI ETLs were used for comparison. OSCs using PEI ETL achieved good operational stability. However, it degraded quickly during air storage. In contrast, the device with ZnO ETL degraded quickly under continuous illumination, while showed relatively better storage stability. Therefore, we used ZnO:PEI composite ETL to improve the performance, and make a balance between the shelf and operational stability for the non-fullerene solar cells. With ZnO:PEI composite ETL, we get excellent operational and shelf stability, with around 80% and 60% performance after 1200 h continuous illumination, and air storage, respectively.

2. Experimental section

2.1. Materials

PEI was purchased from Sigma-Aldrich. The weight-average molecular weight (Mw) of the PEI is about 25 kDa and the number-average molecular weight (Mn) is about 10 kDa. ZnO was prepared in our laboratory according to previous work [30]. Polymer PM6 (PBDB-T-2F) and Y6 were purchased from Organtec.

2.2. Fabrication of OSCs

Organic solar cells with the structure of ITO/ETL (pure ZnO/pure PEI/ZnO:PEI)/PM6:Y6/MoO_3/Al (as showed in Fig. 1(a)) were fabricated. ITO glasses were successively ultrasonic cleaned by deionized water, acetone and isopropanol, then stored in isopropanol. When fabrication, ITO glasses were dried by nitrogen flow and UV ozone treatment for 30 min. The electron transfer layer was spin-coated on ITO glass and annealed at 130 °C for 10 min. The concentration of the ZnO nanoinks was 15 mg/mL. PEI was dissolved in methanol and the concentration was 0.4 mg/mL. ZnO:PEI composite material contained 0.5 mg/mL PEI and 15 mg/mL ZnO in methanol solution. The active layer was spin coated on the top of ETLs by a sequential deposition method [31–33]. This method could effectively control the morphology and phase separation of the active layer. The active layer was annealed at 100 °C for 10 min. After that, 20 nm MoO_3 and 100 nm Al were fabricated by thermal evaporation. The effective area of the devices was 0.09 cm^2.

Table 1
Performance of PM6:Y6 devices with ZnO, PEI and ZnO:PEI as ETL.

ETL	V_{OC} (V)	J_{SC} (mA/cm^2)	FF	PCE (%)[a]	Rs (Ω*cm^2)	Rsh (Ω*cm^2)
ZnO	0.84 (0.84 ± 0.01)	25.84	0.70 (0.70 ± 0.01)	15.20 (15.12 ± 0.08)	3.8	1275
PEI (0.04 mM)	0.84 (0.84 ± 0.01)	26.29	0.69 (0.69 ± 0.01)	15.24 (15.18 ± 0.06)	4.2	1218
PEI (0.1 mM)	0.82 (0.82 ± 0.01)	24.58	0.64 (0.64 ± 0.01)	12.96 (12.54 ± 0.26)	7.5	799
ZnO:PEI (0.02 mM)	0.84 (0.84 ± 0.01)	25.90	0.69 (0.69 ± 0.01)	15.12 (14.99 ± 0.12)	3.5	1034
ZnO:PEI (0.05 mM)	0.84 (0.84 ± 0.01)	26.96	0.70 (0.70 ± 0.01)	15.85 (15.80 ± 0.05)	3.6	1212
ZnO:PEI (0.07 mM)	0.84 (0.84 ± 0.01)	26.09	0.70 (0.70 ± 0.01)	15.27 (15.20 ± 0.09)	3.6	950
ZnO:PEI (0.1 mM)	0.84 (0.84 ± 0.01)	25.62	0.70 (0.70 ± 0.01)	15.06 (14.89 ± 0.17)	3.6	1021

[a] The average performance was calculated from 8 individual devices.

2.3. Characterization

All characterizations of OSCs were measured without encapsulation. Digital source meter (Keithley, model 2400, USA) was used to test current density-voltage (*J-V*) characteristics of OSCs at a light intensity of 100 mW/cm^2 by Xenon-arc-lamp-based solar simulator (Zolix SS150, China). External quantum efficiencies (EQE) were measured under one sun operation conditions. An electrochemical workstation (Metrohm Autolab PGSTAT 302 N, The Netherlands) was applied to test impedance spectra. An ultraviolet–visible spectrophotometer (PerkinElmer Lambda 750, USA) was employed to characterize the absorption spectra of Y6/ETL layer. Operational stabilities were measured at maximum power point in the glove box ($H_2O < 10$ ppm, $O_2 < 10$ ppm) under continuously illuminated with LED white light (D&R Light, LW5300KA-150, Suzhou D&R Instruments). The absorption spectra of the Y6/ETLs films were measured after several hours' continuous illumination. The shelf stabilities of the OSCs and the absorption spectra of the Y6/ETLs films were measured through storing the devices in air environment (25 °C, 35–45%RH) and regularly testing V_{OC}, J_{SC}, FF and PCE.

3. Results and discussion

3.1. Device performance of the ZnO, PEI and ZnO:PEI ETL-based OSCs

The device structure of the ITO/ETL/Active layer/MoO_3/Al inverted OSCs is shown in Fig. 1(a), where ZnO, PEI and ZnO:PEI composite material were used as the ETLs. Molecule chemical structures of PM6, Y6 and PEI (polyethyleneimine) are also shown in Fig. 1(a). ZnO:PEI composite ETL was optimized through regulating the concentration of PEI.

The *J-V* characteristic and EQE curves of the PM6:Y6 devices with different ETLs are shown in Fig. 1(b–d). The detailed performance parameters of those devices are listed in Table 1. As can be seen from the *J-V* and EQE curves, and Table 1, PM6:Y6 based devices with ZnO, PEI and ZnO:PEI ETLs gave nearly identical V_{OC} of 0.84 V. ZnO and ZnO:PEI ETL devices gave a same FF of 0.70, which was slightly higher than that of the PEI based device. Furthermore, ZnO:PEI (0.05 mM) ETL-based device had a J_{SC} of 26.96 mA/cm^2, which was better than 26.29 mA/cm^2 for the PEI ETL-based device and 25.84 mA/cm^2 for the ZnO ETL-based device. The EQE curve of the PM6:Y6 OSCs had a weak sharp peak at about 365 nm and a broad peak at about 400–900 nm. Among the three

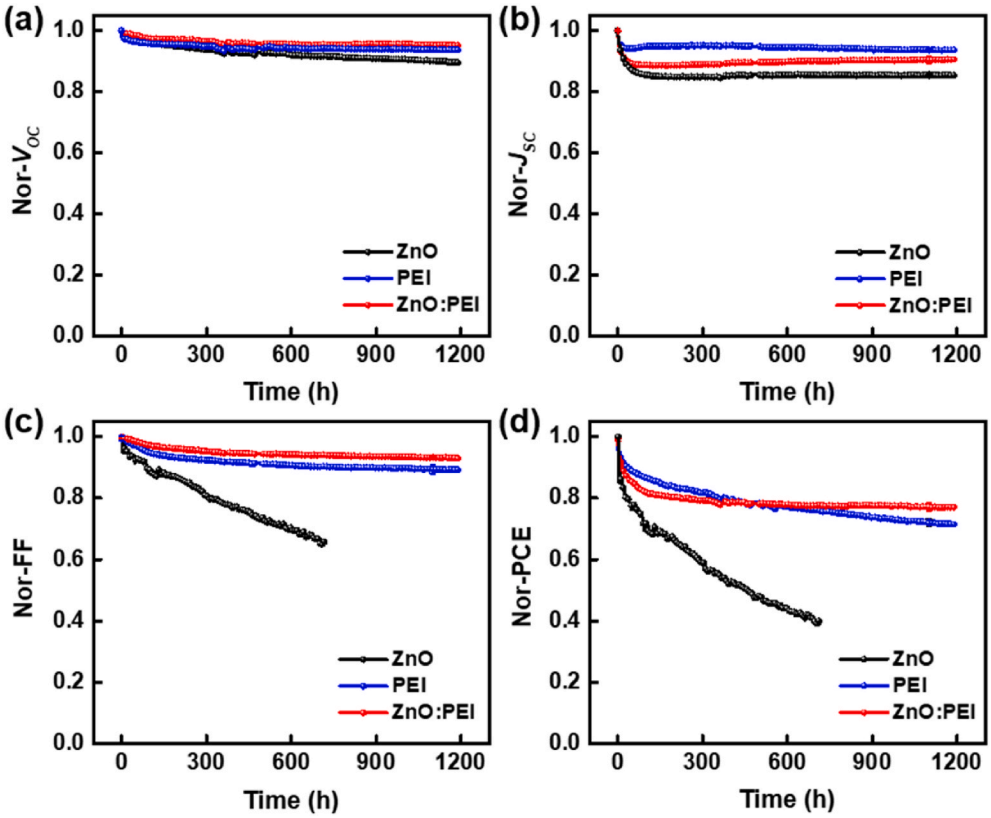

Fig. 2. Normalized (a) V_{OC}, (b) J_{SC}, (c) FF, and (d) PCE decay of the PM6:Y6 solar cells with ZnO, PEI, ZnO:PEI as the ETLs under continuous illumination.

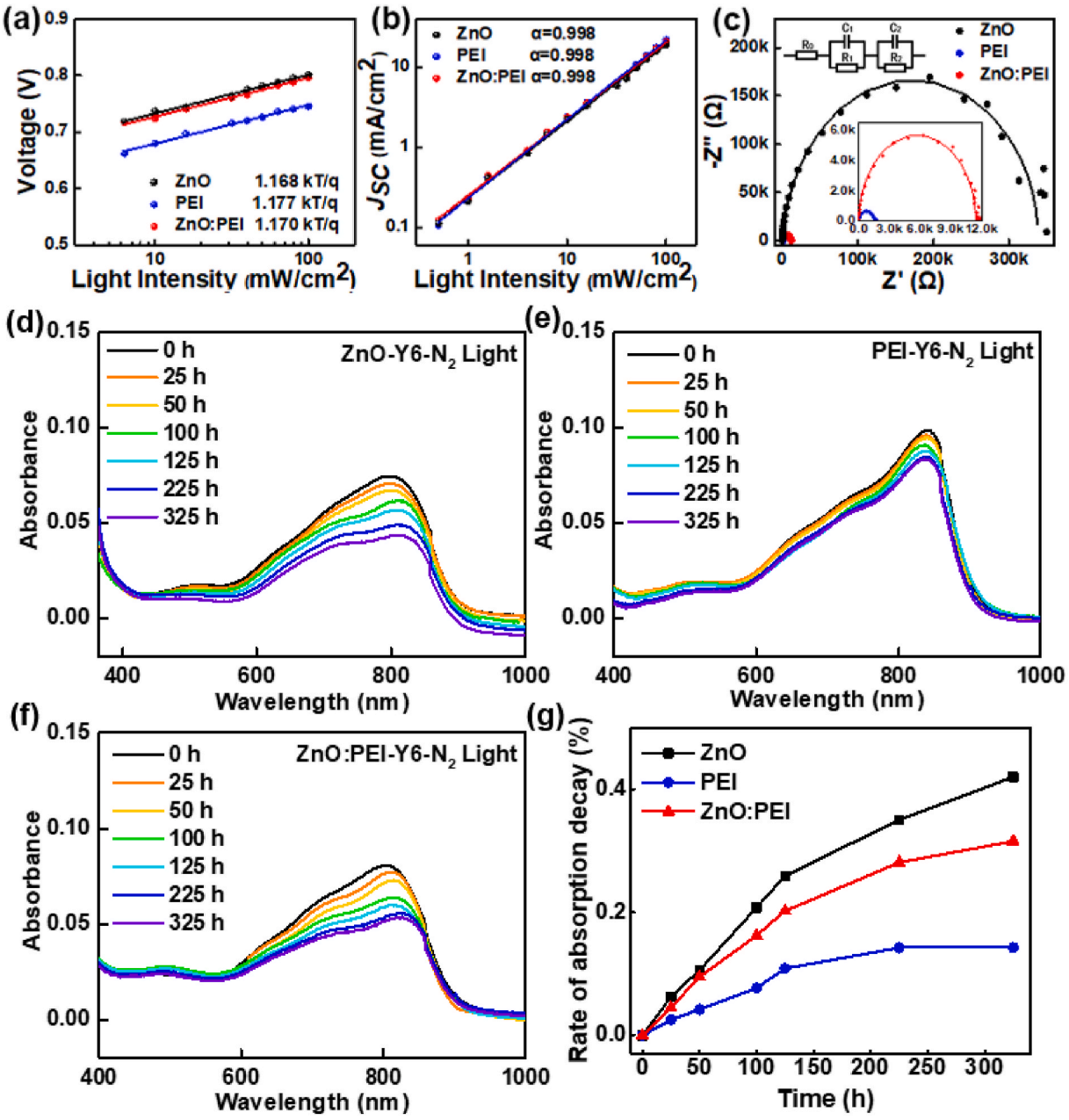

Fig. 3. Light dependence of (a) V_{OC} and (b) J_{SC} (c) Electrochemical impedance spectroscopy (EIS) for aged PM6:Y6 devices in the N_2-filled glove box under light illumination for 1200 h; The UV–vis absorption spectra of (d) ZnO/Y6, (e) PEI/Y6, (f) ZnO:PEI/Y6 films and (g) the absorption decays rate of those films under illumination.

ETLs-based devices, EQE curves of PEI and ZnO:PEI device had wider absorption at 400–500 nm. Therefore, ZnO:PEI (0.05 mM) and PEI ETL based device gave the higher J_{SC}. To explain the difference of J_{SC}, the thickness of the active layers on different ETLs were measured. The results showed similar thickness of PM6:Y6 on different ETLs (115, 117 and 120 nm on ZnO, PEI, and ZnO:PEI ETL, respectively). Meanwhile, the transmittance spectra of the ZnO, PEI and ZnO:PEI films had been tested and showed in Figure S1. It was found that the PEI and ZnO:PEI films showed higher transmittance spectra in the region of 420–470 nm, which would lead to the increase in transmittance of ETL. That was the reason for the higher J_{SC} of the PEI and ZnO:PEI-based device relative to the ZnO device. These results indicated the PEI ETL based devices have the advantage in J_{SC} and ZnO ETL based devices have advantageous in FF. The ZnO:PEI ETL based device with PEI concentration of 0.05 mM showed the highest PCE of 15.85% due to combining the ZnO and PEI as the ETL. In addition, it was meaningful to find that ZnO:PEI composite ETL with 0.1 mM PEI showed a similar efficiency of 15.06%, while device with pure 0.1 mM PEI had V_{OC} of 0.82 V, J_{SC} of 24.58 mA/cm^2, FF of 0.64, PCE of 12.96%. This result revealed that the PEI concentration in ZnO:PEI can be much higher than the pure PEI concentration. The dark *J-V* curves of the PM6:Y6 devices with three ETLs were shown in Fig. 1 (d). Rectification ratio increased from 596 of ZnO ETL device, and 1.2×10^4 of PEI ETL device to 5.4×10^4 of ZnO:PEI ETL device, which would improve the charge selectivity and enhance the device performance.

3.2. *Operational stability of the ZnO, PEI and ZnO:PEI ETL-based devices*

The operational stability of the PM6:Y6 OSCs was measured through aging the devices in the glove box under continuous illumination. Fig. 2 (a–d) exhibits the evolution of V_{OC}, J_{SC}, FF and PCE of these devices. The

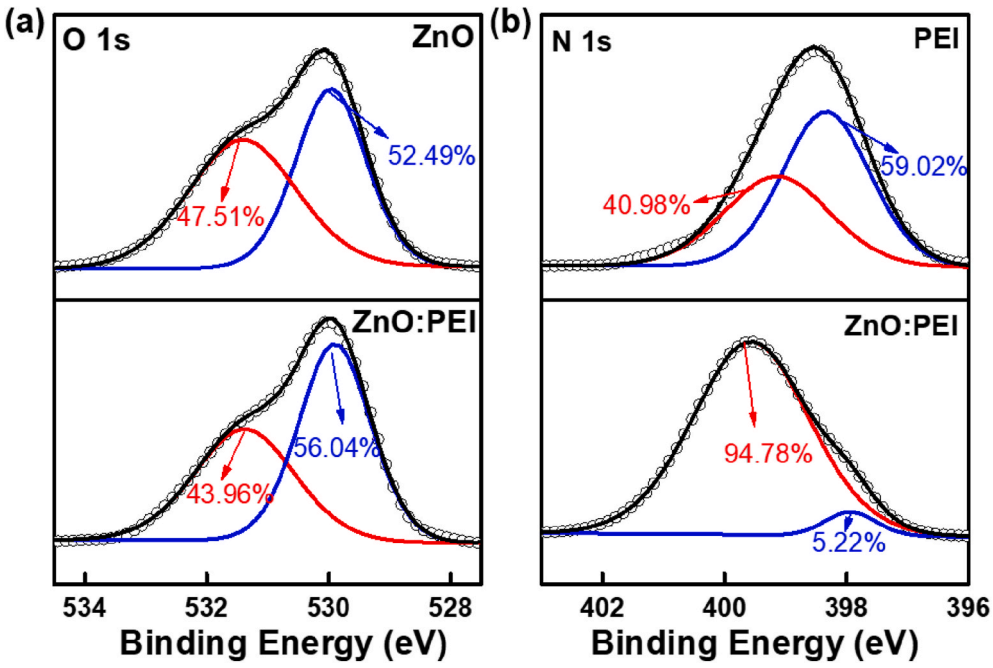

Fig. 4. (a) O 1s core level of the ZnO and ZnO:PEI films and (b) N 1s core level of the PEI and ZnO:PEI films.

devices performance after illumination aging was listed in Table S1. As shown by Fig. 2(a), V_{OC} showed slight degradation during 1200 h aging. For the ZnO, PEI, and ZnO:PEI ETL-based devices, V_{OC} remained 90%, 93% and 94% of the initial value, respectively. As shown by Fig. 2(b), the degradation process of *J*sc contained a fast burn-in degradation and slow degradation process. The ZnO device showed the fastest decay speed for the burn-in degradation process, while the PEI device showed the slowest decay speed. Finally, the J_{SC} of the ZnO, PEI, ZnO:PEI devices were 85%, 90% and 94% of the initial value. For the evolution of FF, PEI and ZnO:PEI-based devices showed a short rapid decay process within 100 h and a slow long time continuous decay after 100 h. During the slow decay step, the FF values were relatively stable. However, the ZnO ETL cells showed a continuous fast decay during the whole aging period. Finally, the normalized FF values of the PEI, and ZnO:PEI devices were 89% and 93%. While the normalized FF value for the ZnO ETL devices decreased to 63% after 750 h. Hence, we found the PCE of the ZnO based device shows a faster degradation at the first 100 h and a relative slow degradation from 100 to 750 h. The first degradation step would be both caused by decay of J_{SC} and FF, and the slow degradation step was mainly due to the decay of FF. As a consequence, the ZnO-based PM6:Y6 device decayed to 40% after 750 h. The evolution of PCE for the PEI and ZnO:PEI-based cells also presented a fast degradation and a slow degradation step. 71% and 80% efficiency were retained after 1200 h.

The light intensity-dependent *J-V* characteristics of the aged devices were measured for further study, as described in Fig. 3. For ideal p-n junction solar cells [34], the V_{OC} and the logarithm of the light intensity are linearly dependent, in which the slope is nk_BT/q. In these parameters, k_B presents the Boltzmann constant, T is absolute temperature, q is the elementary charge, and n is often associated with the trap-assisted recombination. As showed in Fig. 3(a) the n values of the ZnO, PEI, and ZnO:PEI devices were 1.17, 1.18, 1.17, which were very similar. These results indicated that devices after illumination decay had similar trap-assisted recombination. The plots of J_{SC} versus the light intensity are demonstrated in Fig. 3(b). The relationship between J_{SC} and light intensity is $J \propto I^{\alpha}$. α presents the bimolecular recombination degree and the loss of the carrier caused by space charge effects. And α of devices were all about 0.998 with little difference, which suggested bimolecular charge recombination and space charge effects can be ignored.

The electrochemical impedance spectroscopy (EIS) analysis was used to analyze the degeneration devices. The equivalent circuit model and the EIS fitting lines are shown in Fig. 3(c). Detailed data of R_0, R_1, R_2, C_1 and C_2 were listed in Table S2. R_0 revealed resistance of electrodes and wires. R_1 and C_1 came from the interface junction [35]. R_2 and C_2 came from bulk-heterojunction (BHJ). According to Table S2, after 1200 h of illumination, R_1 of ZnO, PEI and ZnO:PEI-based devices is 6909, 1583 and 5439 Ω, indicated the PEI-based device has smaller interface contact resistance. R_2 of ZnO, PEI and ZnO:PEI ETL-based devices was 331,700, 9633 and 5962 Ω, respectively. R_2 of the ZnO ETL-based devices was extremely higher than those of PEI and ZnO:PEI, which may indicate the serious degradation in the active layer and cause the loss of exciton transport in ZnO-based devices.

It was previously reported that the degradation of organic acceptor materials at the interface of ZnO is the main reason of poor stability in non-fullerene acceptor based OSCs due to the photocatalysis of ZnO [12]. And it was demonstrated that the long-term stability of OSCs was improved by modifying ZnO ETL. To further clarify the degradation characteristics, the evolution of the UV–vis spectra of the ZnO/Y6, PEI/Y6 and ZnO:PEI/Y6 films during the continuous illumination was measured. Fig. 3(d–g) shows the evolution of the UV–vis spectra of the ZnO/Y6, PEI/Y6 and ZnO:PEI/Y6 films after 325 h illumination. The absorption peak of the Y6 film at 800 nm was recorded. Frist, it should be clarified that the initial absorption intensity of Y6 on the PEI ETL is stronger than the films on the ZnO and ZnO:PEI ETLs, shown in Figure S2(a). However, the absorption intensity of Y6 in the PM6:Y6 blend films was nearly the same on the different ETLs (Figure S2(b)). These results indicated different adhesion between Y6 and different ETLs, but similar adhesion of the PM6:Y6 blend solution with different ETLs. As showed by the evolution of the absorption spectra, we found the absorbance of the Y6 component gradually decreases during continuous illumination. Particularly, the absorption of the Y6 component of the ZnO/Y6 film showed an obvious decrease. In contrast, a slight change was observed in the PEI/Y6 film. It is worth mentioning that the decay of the acceptor under light and air is negligible (Figure S3). Thus, the gradual decrease of the absorption spectra of Y6 was caused by interface degradation. Besides, A_0 was initial absorption, t was the illumination time and A_t was absorption after t hours illumination. The decay rate was calculated using an equation of $(A_0\text{-}A_t)/A_0$, and the dependence of decay rate on time was plotted in Fig. 3(g). It is

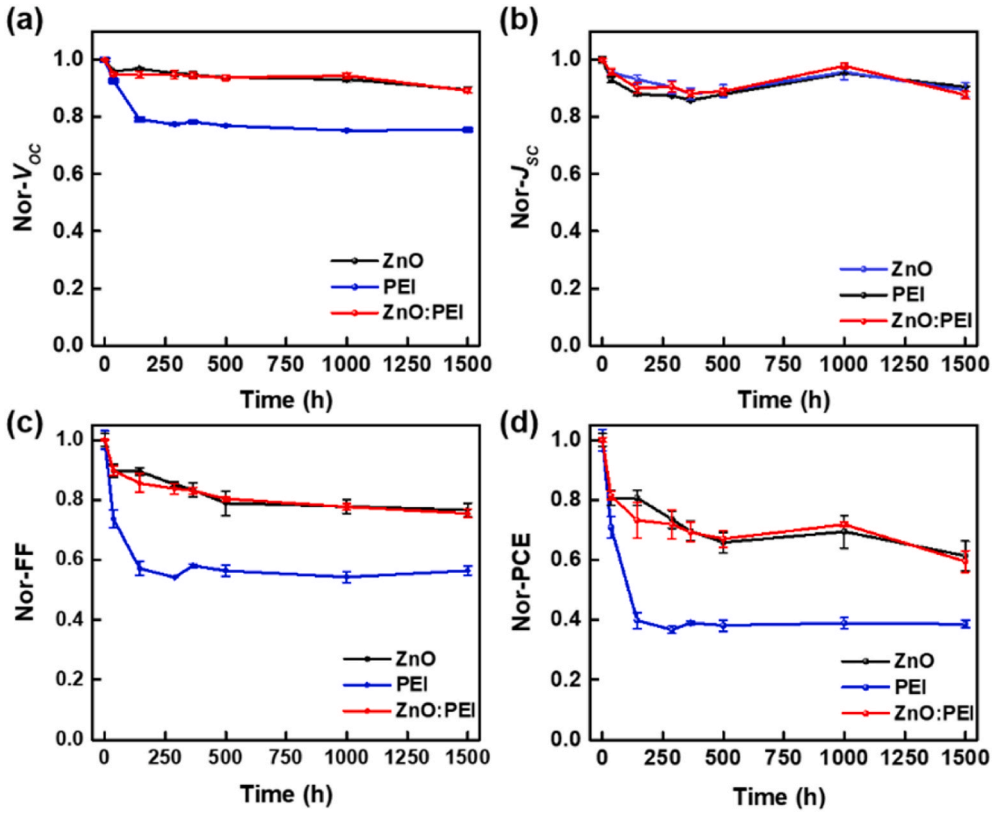

Fig. 5. Normalized (a) V_{OC}, (b) J_{SC}, (c) FF, and (d) PCE decay of the PM6:Y6 solar cells with ZnO, PEI, ZnO:PEI as the ETLs stored in the air with room temperature a relative humidity of around 30%.

indicated that the decay rate of absorption in ZnO/Y6 was the fastest, and the decay rate of absorption in PEI/Y6 was the slowest. Also, the decay speed was fast in the first 100 h and slow from 100 to 300 h. This change trend of absorption decay for Y6/ETLs was similar to the degradation of devices performance under illumination. And the decay rate of absorption induced by the photocatalysis of ZnO can be slowed down by doping PEI into the ZnO ETL. A similar phenomenon was reported in previous works where Zn atoms in ZnO films could be chelated with the incorporation of PEI [25].

We deeply explored the operational stability mechanism from the aspects of the component and defects of ZnO films. The X-ray photoelectron spectroscopy (XPS) spectra of ZnO and ZnO:PEI films had been investigated to characterize the films surface properties. Fig. 4(a) presents the XPS spectra of O 1s of ZnO and ZnO:PEI films. The O ls core level peaks were composed of two peaks. The peak at 530 eV came from the lattice oxygen of ZnO, and binding energy of 531.5 eV XPS peak corresponded to adsorbed oxygen and oxygen defects on the surface of the ZnO films. In comparison with the ZnO films, the count of absorbed oxygen in ZnO:PEI films decreased from 47.51% to 43.96%. And Fig. 4 (b) shows the XPS spectra of N 1s of PEI and ZnO:PEI films. The binding energy of 400 eV peak corresponded to the protonated nitrogen, and peak at 398 eV was attributed to neutral state. When composited with ZnO, the content of 400 eV binding energy of N atoms increased to 94.78%, suggesting more nitrogen protonated. This result showed that the adsorbed oxygen defection of ZnO film could been passivated with the composition of PEI, which was consistent with the previous result [24]. Therefore, the operational stability of ZnO:PEI cells was improved relative to the ZnO device.

3.3. Shelf stability of the ZnO, PEI and ZnO:PEI ETL-based devices

Fig. 5 depicts the performance decay curves of devices with different electron transporting layers in the air and dark environment without encapsulation. OSCs were stored in an air environment (25 °C, 35–45% RH) without illumination, and the *J-V* characteristics of the devices were measured at different time. Detail device performance after aging was shown in Table S3. PEI ETL-based devices displayed 80% loss of V_{OC} and 60% loss of FF at the first 175 h. These losses resulted in the deadly degradation of PCE. Only 40% efficiency of the intimal value remained. From 175 to 1500 h, the device performance kept relatively stable. Whatever, typical "S" shape was observed in the *J-V* curves (as showed in Figure S4). Thus, the device performance was very low. In contrast, ZnO and ZnO:PEI devices showed relatively stable V_{OC} and J_{SC}. FF continuously decayed to 80% of the initial value. Consequently, normalized PCE values of ZnO and ZnO:PEI could both remain above 60%. These results showed the PEI-based device showed a poor shelf device relative to the ZnO device. But, using the ZnO:PEI composite ETL, a comparable lifetime as the ZnO device could be obtained.

The interface combination in the aged devices was analyzed using the light intensity-dependent *J-V* curves and the EIS spectra as Fig. 6 (a–c), n corresponded to ZnO, PEI, ZnO:PEI based devices after air stability test were 1.56, 1.82 and 1.79, respectively, indicating that after air decay, ZnO based devices owned the lowest trap-assisted recombination degree. From the plots of J_{SC} versus the light intensity, α around 1 in these ETLs-based devices, suggesting bimolecular charge recombination and space charge effects are negligible as well. As showed in Table S4, these devices presented similar R_2 and C_2, but quite different R_1 and C_1. Specifically, after 1500 h of air decay, the PEI-based devices showed a R_1 of 66,450 Ω, which was much larger than 3755 and 2757 Ω. But the corresponding R_2 was in the same order of magnitude as others. Such a result implied interface degradation might be the main degradation reason for the PEI-based devices.

At the same time, the evolution of the absorption spectrum degeneration of the Y6 films during long-term storage in air (25 °C, 45%RH) was also measured. As shown in Fig. 6(d–g), it was found the absorption intensity of the Y6 films on different ETLs also gradually decreased as

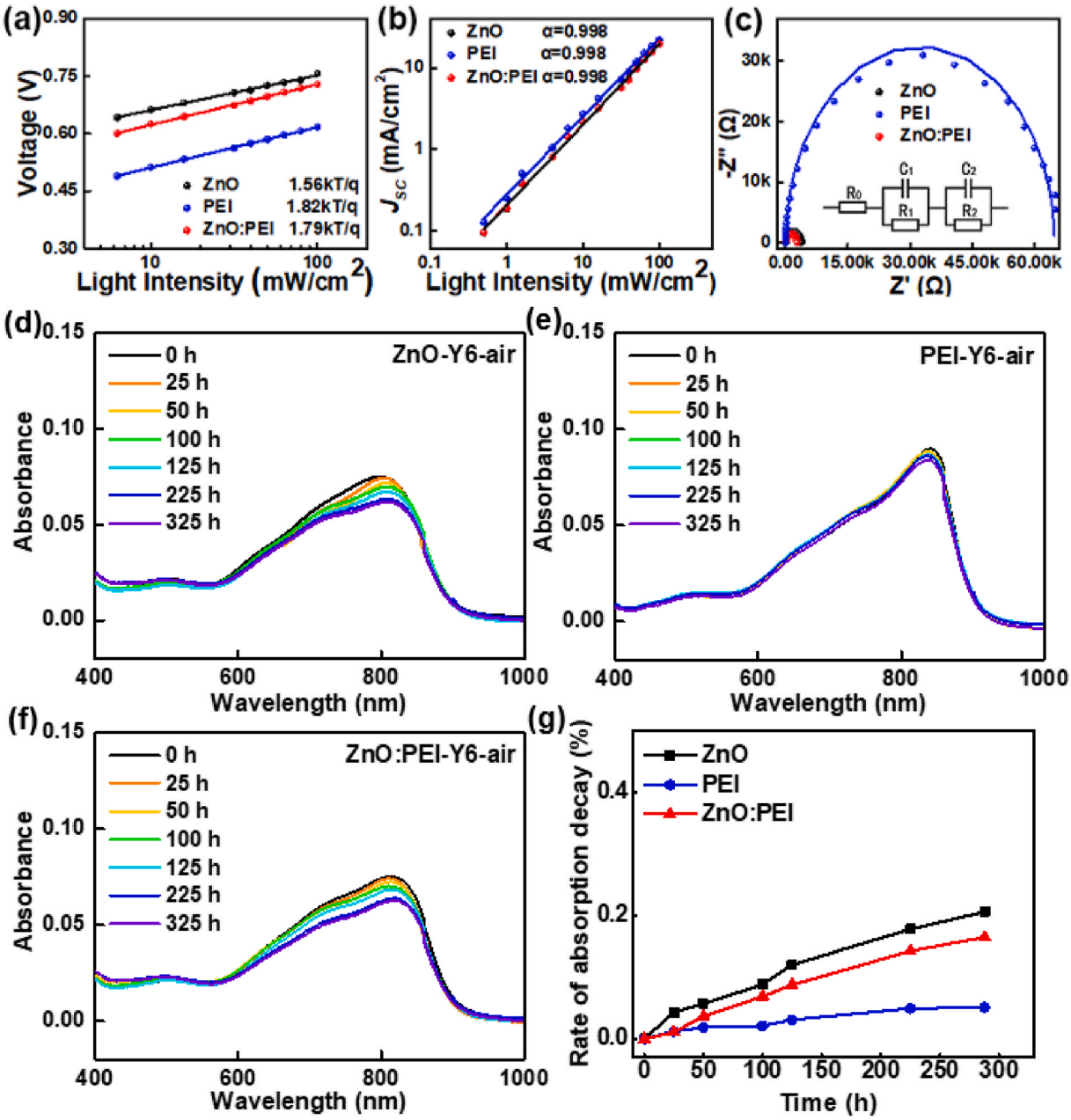

Fig. 6. Light intensity dependence of (a) V_{OC} and (b) J_{SC} and (c) Electrochemical impedance spectroscopy (EIS) for the aged PM6:Y6 devices with different ETLs after storage in the dark air environment for 1500 h; The UV–vis absorption spectra of (d) ZnO/Y6, (e) PEI/Y6, (f) ZnO:PEI/Y6 films stored in the air at room temperature a relative humidity of 40 ± 5% and (g) the absorption decay curves of corresponding to those films.

storage in dark air conditions, indicating the degradation of Y6 molecular. Nevertheless, the decline speed was much slower than the films during continuous illumination (as shown in Fig. 6(g)). Among the films on different ETLs, the degradation speed of the ZnO/Y6 films was the fastest, and that of the PEI/Y6 films was the slowest. Such a result was in agreement with the case of continuous illumination, while inconsistent with device shelf degradation. Particularly, the PEI ETL based device degraded fastest in air, whereas decrease of the absorption intensity was the smallest. Thus, we could make a reasonable speculation that the degradation of Y6 molecular was not the critical reason for device degradation during air storage. Herein, it was interesting to find the similar decomposition of Y6 on ZnO films during storage in the dark air, indicated the interface degradation between Y6 and ZnO was not only caused by the photocatalysis effect of ZnO. In our previous work, we demonstrated the existence of surface hydroxy on the ZnO was the original interface degradation of the non-fullerene acceptor [12,36]. When stored in air, more hydroxy groups would be absorbed on the surface of ZnO because of moisture, which might accelerate such degradation. Therefore, we could make a speculation that both photocatalysis effect and direct chemical reaction would occur between ZnO and the non-fullerene acceptor, and the former and later took responsibility for operational degradation and shelf degradation, respectively. But the photocatalysis degradation was much faster.

To see the insight of the degradation mechanism of the PEI-based device in air, we designed an aging step to the ITO/ETL for 750 h in the air (25 °C, 35–45%RH). After that, the active layer, MoO_3 and Al were deposited on three different electron transport layers to form the devices. The device performance is showed in Table S5. PEI-based devices gave a V_{OC} of 0.82 V, J_{SC} of 25.57 mA/cm^2, FF of 0.58 and PCE of 12.18%. ZnO-based devices gave a reasonable performance of 14.36%

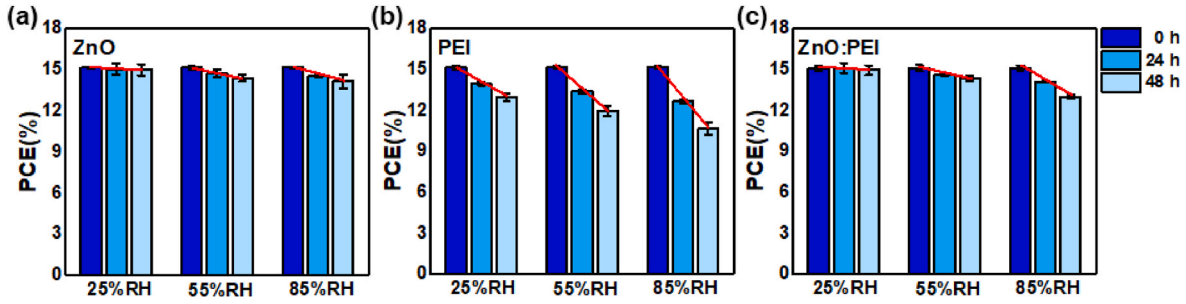

Fig. 7. The PCE losses of different ETLs-based devices in the air with 25% RH, 55% RH and 85% RH.

with V_{OC} of 0.82 V, J_{SC} of 26.67 mA/cm^2, FF of 0.66. The performance of ZnO:PEI-based devices are V_{OC} of 0.82 V, J_{SC} of 26.30 mA/cm^2, FF of 0.67 and PCE of 14.45%.We can see these devices with aged ZnO and ZnO:PEI ETLs gave a similar performance to the devices with fresh-prepared ETLs, unlike the PEI devices. This result proved the degradation of PEI lead to the fast performance decay in air condition, which was because of the hygroscopic of PEI molecular [14,15].

Furthermore, Fig. 7 demonstrates the influence of humidity conditions on the shelf stability of the devices. Three different humidity conditions, *i. e.* 25%RH, 55%RH, and 85%RH were compared. For the ZnO ETL device, the humidity showed a slight influence on the performance, specifically for the case of low humidity condition. Under the condition of 85%RH, the device performance declined 5% after 48 h. Unlike the case of ZnO, the PEI ETL-based device was highly sensitive to humidity. The degradation speed increased greatly with the increase of environmental humidity. For the 25%RH, 55%RH, 85%RH humidity, the performance decreased to 85% (PCE = 13.01%), 80% (PCE = 12.06%), and 71% (PCE = 10.76%). The ZnO:PEI composite ETL device displayed lower humidity sensitivity than PEI devices. Under the 55% RH humidity condition, 94% (PCE = 14.39%) of PCE after 48 h was observed. And as increasing humidity to 85%RH, the PCE of ZnO:PEI composite ETL-based devices remained 86% (PCE = 13.10%).

4. Conclusions

In this work, we compared the shelf and operational stability of the PM6:Y6 solar cells with different ETLs. The results showed the device with ZnO ETL degraded much quickly than the PEI ETL-based device. However, under the air storage condition, the ZnO ETL-based device was much more stable than the PEI ETL-based device. The quick photo-degradation of the ZnO cells was due to the degradation of Y6 due to the photocatalysis effect, and the quick air decay of the PEI-based device was originated from the degradation of PEI. With a composite ETL with ZnO and PEI, synergetic improvement of stability both in the continuous illumination and air storage conditions was achieved. Organic solar cells with ZnO:PEI electron transport layer remained 80% of the original PCE after illumination for 1200 h, and remained above 60% of PCE after 1500 h storage in air.

Declaration of competing interest

The authors declare that they have no known competing financial interests or personal relationships that could have appeared to influence the work reported in this paper.

Acknowledgments

The work is financially supported by the National Natural Science Foundation of China (51773224, 22075315), Youth Innovation Promotion Association, CAS (2019317), the Ministry of Science and Technology of China (2016 YFA0200700), Vacuum Interconnected Nanotech Workstation, Suzhou Institute of Nano-Tech and Nano-Bionics, Chinese Academy of Sciences (CAS).

Appendix A. Supplementary data

Supplementary data to this article can be found online at https://doi.org/10.1016/j.orgel.2021.106257.

References

[1] N. Chaturvedi, N. Gasparini, D. Corzo, J. Bertrandie, N. Wehbe, J. Troughton, D. Baran, All slot-die coated non-fullerene organic solar cells with PCE 11%, Adv. Funct. Mater. 31 (2021) 2009996.
[2] Z. Jiang, F.J. Wang, K. Fukuda, A. Karki, W. Huang, K. Yu, T. Yokota, K. Tajima, T. Q. Nguyen, T. Someya, Highly efficient organic photovoltaics with enhanced stability through the formation of doping-induced stable interfaces, Proc. Natl. Acad. Sci. U.S.A. 117 (2020) 6391–6397.
[3] S.X. Dai, X.W. Zhan, Nonfullerene acceptors for semitransparent organic solar cells, Adv. Energy Mater. 8 (2018) 1800002.
[4] Q. Liu, Y. Jiang, K. Jin, J. Qin, J. Xu, J.X. Wenting Li, Jinfeng Liu, Zuo Xiao, Kuan Sun, Shangfeng Yang, Xiaotao Zhang, Liming Ding, 18% efficiency organic solar cells, Sci. Bull. 65 (2020) 272–275.
[5] L.P. Duan, A. Uddin, Progress in stability of organic solar cells, Adv. Sci. 7 (2020) 1903259.
[6] G.Y. Zhang, J.B. Zhao, P.C.Y. Chow, K. Jiang, J.Q. Zhang, Z.L. Zhu, J. Zhang, F. Huang, H. Yan, Nonfullerene acceptor molecules for bulk heterojunction organic solar cells, Chem. Rev. 118 (2018) 3447–3507.
[7] R. Sorrentino, E. Kozma, S. Luzzati, R. Po, Interlayers for non-fullerene based polymer solar cells: distinctive features and challenges, Energy Environ. Sci. 14 (2021) 180–223.
[8] S.Q. Bi, X.Y. Leng, Y.X. Li, Z. Zheng, X.N. Zhang, Y. Zhang, H.Q. Zhou, Interfacial modification in organic and perovskite solar cells, Adv. Mater. 31 (2019) 1805708.
[9] H. Ma, H.L. Yip, F. Huang, A.K.Y. Jen, Interface engineering for organic electronics, Adv. Funct. Mater. 20 (2010) 1371–1388.
[10] Y.M. Sun, J.H. Seo, C.J. Takacs, J. Seifter, A.J. Heeger, Inverted polymer solar cells integrated with a low-temperature-annealed sol-gel-derived ZnO Film as an electron transport layer, Adv. Mater. 23 (2011) 1679–1683.
[11] Y.Y. Jiang, L.L. Sun, F.Y. Jiang, C. Xie, L. Hu, X.Y. Dong, F. Qin, T.F. Liu, L. Hu, X. S. Jiang, Y.H. Zhou, Photocatalytic effect of ZnO on the stability of nonfullerene acceptors and its mitigation by SnO_2 for nonfullerene organic solar cells, Mater. Horiz. 6 (2019) 1438–1443.
[12] B.W. Liu, Y.F. Han, Z.R. Li, H.M. Gu, L.P. Yan, Y. Lin, Q. Luo, S.F. Yang, C.Q. Ma, Visible light-induced degradation of Inverted polymer:nonfullerene acceptor solar cells: initiated by the light absorption of ZnO Layer, Sol. RRL 5 (2021) 2000638.
[13] S.R. Gollu, R. Sharma, G. Srinivas, S. Kundu, D. Gupta, Incorporation of silver and gold nanostructures for performance improvement in P3HT:PCBM inverted solar cell with rGO/ZnO nanocomposite as an electron transport layer, Org. Electron. 29 (2016) 79–87.
[14] S. Bontapalle, A. Opitz, R. Schlesinger, S.R. Marder, S. Varughese, N. Koch, Electrode work function reduction by polyethylenimine interlayers: choice of solvent and residual solvent removal for superior functionality, Adv. Mater. Interfaces 7 (2020) 2000291.
[15] Y. Zhou, C. Fuentes-Hernandez, J. Shim, J. Meyer, A.J. Giordano, H. Li, P. Winget, T. Papadopoulos, H. Cheun, J. Kim, M. Fenoll, A. Dindar, W. Haske, E. Najafabadi, T.M. Khan, H. Sojoudi, S. Barlow, S. Graham, J.-L. Bredas, S.R. Marder, A. Kahn, B. Kippelen, A universal method to produce low-work function electrodes for organic electronics, Science 336 (2012) 327–332.
[16] L. Yan, Y. Song, Y. Zhou, B. Song, Y. Li, Effect of PEI cathode interlayer on work function and interface resistance of ITO electrode in the inverted polymer solar cells, Org. Electron. 17 (2015) 94–101.
[17] M. Sadeghianlemraski, B.Y. Lee, T. Davidson-Hall, Z. Leonenko, H. Aziz, Enhanced photo-stability of inverted organic solar cells via using polyethylenimine in the electron extraction layers, Org. Electron. 73 (2019) 26–35.
[18] M. Sadeghianlemraski, H. Aziz, Reducing ultraviolet-induced open-circuit voltage loss in inverted organic solar cells by maintaining charge selectivity of the electron collection contact using polyethylenimine, Sol. Energy 198 (2020) 427–433.

[19] L. Hu, S.X. Xiong, W. Wang, L.L. Sun, F. Qin, Y.H. Zhou, Influence of substituent groups on chemical reactivity kinetics of nonfullerene acceptors, J. Phys. Chem. C 124 (2020) 2307–2312.
[20] Y. Wang, B. Jia, F. Qin, Y. Wu, W. Meng, S. Dai, Y. Zhou, X. Zhan, Semitransparent, non-fullerene and flexible all-plastic solar cells, Polymer 107 (2016) 108–112.
[21] M.B. Yi, J.R. Ku, J.S. Yoon, J. Kal, W. Lee, S.G. Oh, Facile preparation of a polymer-ZnO composite colloid as an electron transport layer and its effects on inverted polymer solar cells, J. Phys. Chem. Solid. 145 (2020) 109538.
[22] J.F. Wei, C.J. Zhang, G.Q. Ji, Y.F. Han, I. Ismail, H.Y. Li, Q. Luo, J.L. Yang, C.Q. Ma, Roll-to-roll printed stable and thickness-independent ZnO:PEI composite electron transport layer for inverted organic solar cells, Sol. Energy 193 (2019) 102–110.
[23] N. Wu, Q. Luo, Z.M. Bao, J. Lin, Y.Q. Li, C.Q. Ma, Zinc oxide: conjugated polymer nanocomposite as cathode buffer layer for solution processed inverted organic solar cells, Sol. Energy Mater. Sol. Cells 141 (2015) 248–259.
[24] L. Hu, Y. Jiang, L. Sun, C. Xie, F. Qin, W. Wang, Y. Zhou, Significant enhancement of illumination stability of nonfullerene organic solar cells via an aqueous polyethylenimine modification, J. Phys. Chem. Lett. 12 (2021) 2607–2614.
[25] F. Qin, W. Wang, L. Sun, X. Jiang, L. Hu, S. Xiong, T. Liu, X. Dong, J. Li, Y. Jiang, J. Hou, K. Fukuda, T. Someya, Y. Zhou, Robust metal ion-chelated polymer interfacial layer for ultraflexible non-fullerene organic solar cells, Nat. Commun. 11 (2020) 4508.
[26] M. Gunther, D. Blatte, A.L. Oechsle, S.S. Rivas, A.A. Yousefi Amin, P. Muller-Buschbaum, T. Bein, T. Ameri, Increasing photostability of inverted nonfullerene organic solar cells by using fullerene derivative additives, ACS Appl. Mater. Interfaces 13 (2021) 19072–19084.
[27] L. Zhang, B. Lin, B. Hu, X. Xu, W. Ma, Blade-cast nonfullerene organic solar cells in air with excellent morphology, efficiency, and stability, Adv. Mater. 30 (2018) 1800343.
[28] S. Qu, J. Yu, J. Cao, X. Liu, H. Wang, S. Guang, W. Tang, Highly efficient organic solar cells enabled by a porous ZnO/PEIE electron transport layer with enhanced light trapping, Sci. China Math. 64 (2021) 808–819.
[29] Y. Ge, L. Hu, L. Zhang, Q. Fu, G. Xu, Z. Xing, L. Huang, W. Zhou, Y. Chen, Polyolefin elastomer as the anode interfacial layer for improved mechanical and air stabilities in nonfullerene solar cells, ACS Appl. Mater. Interfaces 12 (2020) 10706–10716.
[30] G. Ji, W. Zhao, J. Wei, L. Yan, Y. Han, Q. Luo, S. Yang, J. Hou, C.-Q. Ma, 12.88% efficiency in doctor-blade coated organic solar cells through optimizing the surface morphology of a ZnO cathode buffer layer, J. Mater. Chem. 7 (2019) 212–220.
[31] K. Weng, L. Ye, L. Zhu, J. Xu, J. Zhou, X. Feng, G. Lu, S. Tan, F. Liu, Y. Sun, Optimized active layer morphology toward efficient and polymer batch insensitive organic solar cells, Nat. Commun. 11 (2020) 2855.
[32] Y. Wang, X. Wang, B. Lin, Z. Bi, X. Zhou, H.B. Naveed, W.M.K. Zhou, Achieving balanced crystallization kinetics of donor and acceptor by sequential-blade coated double bulk heterojunction organic solar cells, Adv. Energy Mater. 10 (2020) 2000826.
[33] Y. Song, K. Zhang, S. Dong, R. Xia, F. Huang, Y. Cao, Semitransparent organic solar cells enabled by a sequentially deposited bilayer structure, ACS Appl. Mater. Interfaces 12 (2020) 18473–18481.
[34] L.P. Yan, J.D. Yi, Q. Chen, J.Y. Dou, Y.Z. Yang, X.G. Liu, L.W. Chen, C.Q. Ma, External load-dependent degradation of P3HT:$PC_{61}BM$ solar cells: behavior, mechanism, and method of suppression, J. Mater. Chem. 5 (2017) 10010–10020.
[35] E.-P. Yao, C.-C. Chen, J. Gao, Y. Liu, Q. Chen, M. Cai, W.-C. Hsu, Z. Hong, G. Li, Y. Yang, The study of solvent additive effects in efficient polymer photovoltaics via impedance spectroscopy, Sol. Energy Mater. Sol. Cells 130 (2014) 20–26.
[36] Y. Han, H. Dong, W. Pan, B. Liu, X. Chen, R. Huang, Z. Li, F. Li, Q. Luo, J. Zhang, Z. Wei, C.-Q. Ma, An efficiency of 16.46% and a t_{80} lifetime of over 4000 h for the PM6:Y6 inverted organic solar cells enabled by surface acid treatment of the zinc oxide electron transporting layer, ACS Appl. Mater. Interfaces 13 (2021) 17869–17881.